Polycyclic Aromatic Hydrocarbons with Aliphatic Sidegroups: Intensity Scaling for the C–H Stretching Modes and Astrophysical Implications

X. J. Yang[1,2], Aigen Li[2], R. Glaser[3], and J. X. Zhong[1]

[1] Department of Physics, Xiangtan University, 411105 Xiangtan, Hunan Province, China; xjyang@xtu.edu.cn, jxzhong@xtu.edu.cn
[2] Department of Physics and Astronomy, University of Missouri, Columbia, MO 65211, USA; lia@missouri.edu
[3] Department of Chemistry, University of Missouri, Columbia, MO 65211, USA; glaserr@missouri.edu

Abstract

The so-called unidentified infrared emission (UIE) features at 3.3, 6.2, 7.7, 8.6, and 11.3 μm ubiquitously seen in a wide variety of astrophysical regions are generally attributed to polycyclic aromatic hydrocarbon (PAH) molecules. Astronomical PAHs may have an aliphatic component, as revealed by the detection in many UIE sources of the aliphatic C–H stretching feature at 3.4 μm. The ratio of the observed intensity of the 3.4 μm feature to that of the 3.3 μm aromatic C–H feature allows one to estimate the aliphatic fraction of the UIE carriers. This requires knowledge of the intrinsic oscillator strengths of the 3.3 μm aromatic C–H stretch ($A_{3.3}$) and the 3.4 μm aliphatic C–H stretch ($A_{3.4}$). Lacking experimental data on $A_{3.3}$ and $A_{3.4}$ for the UIE candidate materials, one often has to rely on quantum-chemical computations. Although the second-order Møller–Plesset (MP2) perturbation theory with a large basis set is more accurate than the B3LYP density functional theory, MP2 is computationally very demanding and impractical for large molecules. Based on methylated PAHs, we show here that, by scaling the band strengths computed at an inexpensive level (e.g., B3LYP/6-31G*), we are able to obtain band strengths as accurate as those computed at far more expensive levels (e.g., MP2/6-311+G(3df,3pd)). We calculate the model spectra of methylated PAHs and their cations excited by starlight of different spectral shapes and intensities. We find that $(I_{3.4}/I_{3.3})_{\rm mod}$, the ratio of the model intensity of the 3.4 μm feature to that of the 3.3 μm feature, is insensitive to the spectral shape and intensity of the exciting starlight. We derive a straightforward relation for determining the aliphatic fraction of the UIE carriers (i.e., the ratio of the number of C atoms in aliphatic units $N_{\rm C,ali}$ to that in aromatic rings $N_{\rm C,aro}$) from the observed band ratios $(I_{3.4}/I_{3.3})_{\rm obs}$: $N_{\rm C,ali}/N_{\rm C,aro} \approx 0.57 \times (I_{3.4}/I_{3.3})_{\rm obs}$ for neutrals and $N_{\rm C,ali}/N_{\rm C,aro} \approx 0.26 \times (I_{3.4}/I_{3.3})_{\rm obs}$ for cations.

Key words: dust, extinction – ISM: lines and bands – ISM: molecules

1. Introduction

The infrared (IR) spectra of a wide range of galactic and extragalactic objects with associated dust and gas are dominated by a series of emission features at 3.3, 6.2, 7.7, 8.6, 11.3, and 12.7 μm (see Peeters 2014). Collectively known as the "unidentified" IR emission (*IUE*) features, due to the fact that the exact nature of their carriers remains unknown (see Peeters et al. 2004; Yang et al. 2017), the hypothesis of polycyclic aromatic hydrocarbon (PAH) molecules as the carriers of the unidentified infrared emission (UIE) features has gained widespread acceptance and extreme popularity. The PAH hypothesis attributes the UIE features to the stretching and bending vibrational modes of PAH molecules (Léger & Puget 1984; Allamandola et al. 1985).

While PAH is a precisely defined chemical term (i.e., PAHs are fused benzene rings made up of carbon and hydrogen atoms), the PAH hypothesis does not really postulate that astronomical PAHs are pure aromatic compounds as strictly defined by chemists. Instead, PAH molecules in astronomical environments may include ring defects (e.g., see Yu & Nyman 2012), substituents (e.g., N in place of C, see Hudgins et al. 2005, Mattioda et al. 2008, Alvaro Galué et al. 2010, Gao et al. 2016; Gruet et al. 2016; O in place of C, see Bauschlicher 1998 Fe in place of C, see Szczepanski et al. 2006; Bauschlicher 2009; Simon & Joblin 2010), partial deuteration (e.g., see Allamandola et al. 1989; Hudgins et al. 2004; Peeters et al. 2004; Draine 2006; Onaka et al. 2014); partial dehydrogenation (e.g., see Tielens et al. 1987; Malloci et al. 2008), and sometimes

superhydrogenation (e.g., see Bernstein et al. 1996; Thrower et al. 2012; Sandford et al. 2013).

Astronomical PAHs may likely also include an aliphatic component, as revealed by the detection in many UIE sources of a weak satellite emission feature at 3.4 μm that always accompanies the 3.3 μm emission feature (e.g., see Geballe et al. 1985, 1989; Jourdain de Muizon et al. 1986, 1990; Nagata et al. 1988; Allamandola et al. 1989; Sandford 1991; Joblin et al. 1996; Sloan et al. 1997). For illustration, in Figure 1 we show the 3.3 and 3.4 μm emission features of several representative astrophysical regions. The 3.4 μm feature is generally thought to arise from the C–H stretching vibration of aliphatic hydrocarbon materials, while the 3.3 μm feature is due to the C–H stretching mode of aromatic hydrocarbons. Also detected in some UIE sources are the aliphatic C–H deformation bands at 6.85 and 7.25 μm (see Sloan et al. 2014, and see Table 3 in Yang et al. 2016a for a summary).

In recent years, the aliphatic fraction of the UIE carriers—the ratio of the number of C atoms in aliphatic units ($N_{\rm C,ali}$) to that in aromatic rings ($N_{\rm C,aro}$)—has received much attention (e.g., see Kwok & Zhang 2011; Li & Draine 2012; Rouillé et al. 2012; Steglich et al. 2013; Yang et al. 2013, 2016a, 2016b). Kwok & Zhang (2011) argued that the material responsible for the UIE features may have a substantial aliphatic component and therefore, by definition, PAHs cannot be the UIE carrier. This argument can be tested by examining the ratio of the observed intensity of the 3.3 μm feature ($I_{3.3}$) to that of the 3.4 μm feature ($I_{3.4}$) of UIE sources. If the intrinsic oscillator strengths (per chemical bond) of the 3.3 μm aromatic
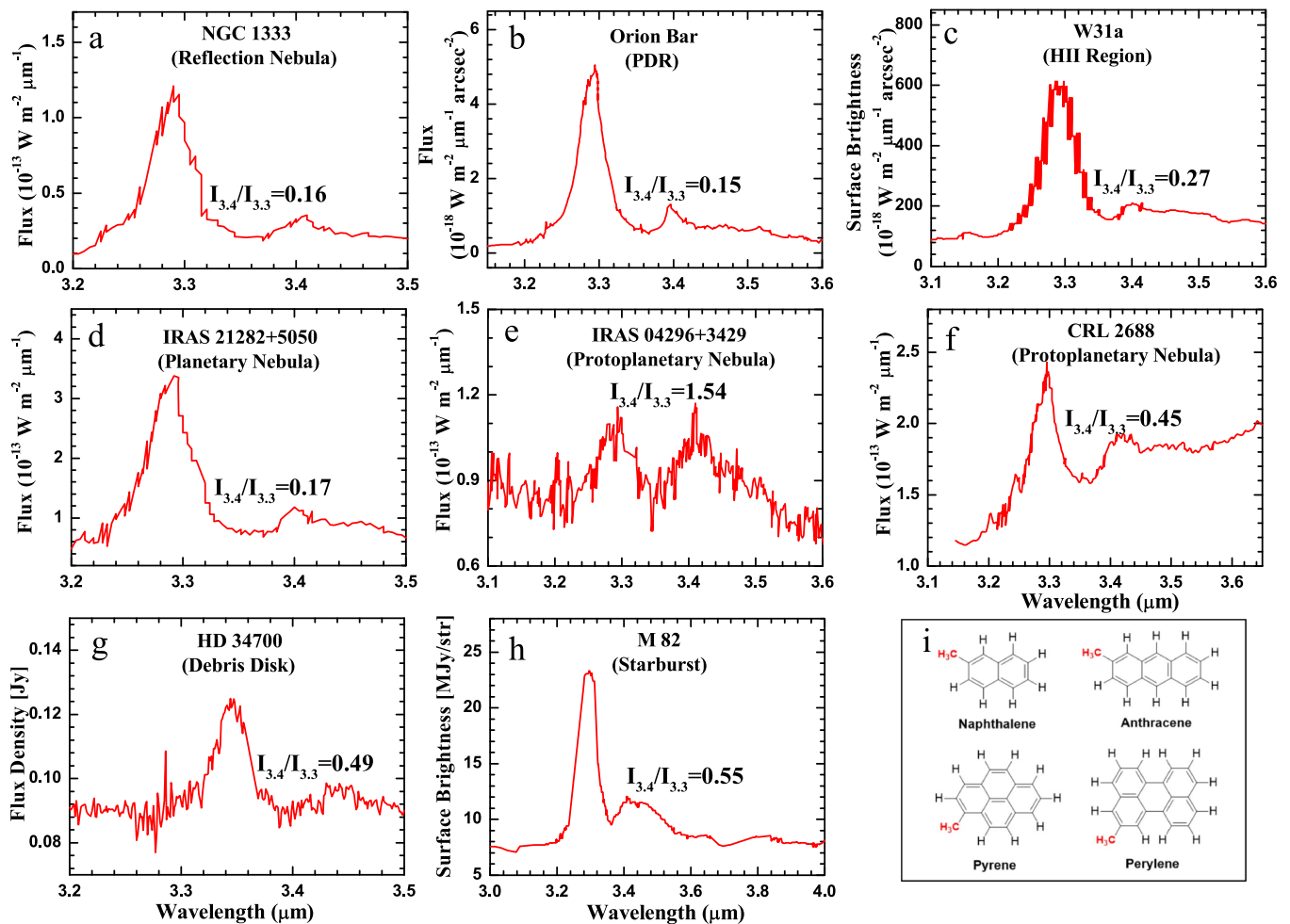
Figure 1. Aromatic and aliphatic C–H stretching emission features seen in representative astronomical sources: (a) NGC 1333 (reflection nebula, Joblin et al. 1996), (b) Orion Bar (photodissociated region [PDR], Sloan et al. 1997), (c) W31a (H II region, Mori et al. 2014), (d) IRAS 21282+5050 (planetary nebula, Nagata et al. 1988), (e) IRAS 04296+3429 (protoplanetary nebula, Geballe et al. 1992), (f) CRL 2688 (protoplanetary nebula, Geballe et al. 1992), (g) HD 34700 (debris disk, Smith et al. 2004), (h) M 82 (starburst galaxy, Yamagishi et al. 2012), and (i) four methylated PAH molecules.

C–H stretch ($A_{3.3}$) and the 3.4 μm aliphatic C–H stretch ($A_{3.4}$) are known, one could drive the aliphatic fraction of the UIE carriers from $N_{C,ali}/N_{C,aro} \approx 0.3 \times (I_{3.4}/I_{3.3}) \times (A_{3.3}/A_{3.4})$ (see Li & Draine 2012). Here the factor 0.3 arises from the assumption of one aliphatic C atom corresponding to 2.5 aliphatic C–H bonds (intermediate between methylene –CH_2 and methyl –CH_3) and one aromatic C atom corresponding to 0.75 aromatic C–H bond (intermediate between benzene C_6H_6 and coronene $C_{24}H_{12}$).

Unfortunately, there is little experimental information on $A_{3.3}$ and $A_{3.4}$ for the UIE candidate materials. Therefore, one often has to rely on quantum-chemical computations based on density functional theory or second-order perturbation theory. To this end, one often uses the Gaussian09 software (Frisch et al. 2009) and employs the hybrid density functional theoretical method (B3LYP) in conjunction with a variety of basis sets. In the order of increasing accuracy and computational demand, the commonly adopted basis sets are (see Pople et al. 1987): 6-31G*, 6-31+G*, 6-311+G*, 6-311G**, 6-31+G**, 6-31++G**, 6-311+G**, 6-311++G**, 6-311+G(3df,3pd), and 6-311++G(3df,3pd). One also often employs second-order Møller–Plesset perturbation theory (hereafter abbreviated as MP2) in conjunction with these basis sets. The MP2 method is thought to be more accurate in computing band intensities than B3LYP (see Cramer 2004).

Indeed, as demonstrated in Section 2, the IR intensities calculated at the B3LYP/6-31G* level for the 3.3 μm aromatic C–H stretches of benzene, naphthalene, anthracene, pyrene, and coronene are much higher compared to their gas-phase experimental results. This is also true for methylated species (e.g., methylated benzene or toluene, see Section 2). Using better basis sets in conjunction with the B3LYP method, we find that the IR intensities still differ by a factor of ~30% compared to the experimental results. In contrast, Pavlyuchko et al. (2012) reported that the IR intensities calculated for benzene and toluene at the level MP2/6-311G(3df,3pd) would match the experimental results very well.

Ideally, in order to compute $A_{3.3}$ and $A_{3.4}$ as accurately as possible, one should study the candidate UIE carriers at the most pertinent levels (e.g., MP2 in conjunction with 6-311++G**, 6-311+G(3df,3pd), or 6-311++G(3df,3pd)). However, the huge computational demand required by these techniques often makes it impractical to compute $A_{3.3}$ and $A_{3.4}$, particularly for large molecules. In this work, based on methylated aromatic hydrocarbon molecules (with the methyl group taken to represent the aliphatic component of the UIE carriers), we present in Section 3 an intensity scaling approach which, by scaling the intensities computed at an inexpensive level (e.g., B3LYP/6-31G*) we are able to obtain intensities as accurate as those computed at far more

expensive levels (e.g., MP2/6-311+G(3df,3pd)). In Section 4 we calculate the model emission spectra of PAHs containing various numbers of methyl sidegroups, excited by starlight of different spectral shapes and intensities. We derive $(I_{3.4}/I_{3.3})_{\mathrm{mod}}$, the ratio of the model intensity of the 3.4 μm feature to that of the 3.3 μm feature. We explore the variation of $(I_{3.4}/I_{3.3})_{\mathrm{mod}}$ with the spectral shape and intensity of the exciting starlight. We summarize the principal results in Section 5.

2. B3LYP IR Intensities for C–H Stretching Modes

To derive the intrinsic oscillator strengths of the 3.3 μm aromatic C–C stretch ($A_{3.3}$) and the 3.4 μm aliphatic C–H stretch ($A_{3.4}$), we have employed density functional theory and second-order perturbation theory to compute the IR vibrational spectra of seven PAH species (benzene C_6H_6, naphthalene $C_{10}H_8$, anthracene $C_{14}H_{10}$, phenanthrene $C_{14}H_{10}$, pyrene $C_{16}H_{10}$, perylene $C_{20}H_{12}$, and coronene $C_{24}H_{12}$), as well as all of their methyl derivatives (see Yang et al. 2013). All of the molecules have been studied in all conformations at the B3LYP/6-31G* level. The calculations always show three methyl C–H stretches for all the methyl derivatives of all the molecules, and we always describe these three bands as $\nu_{\mathrm{Me,1}}$, $\nu_{\mathrm{Me,2}}$, and $\nu_{\mathrm{Me,3}}$.

For benzene, the gas-phase experimental spectrum of the *National Institute of Standards and Technology* (NIST)[4] gives an absorption intensity of $\sim$54.4 km mol^{-1} for the aromatic C–H stretches, in close agreement with the intensity of $\sim$55 km mol^{-1} computed by Pavlyuchko et al. (2012) at the MP2/6-311G (3df,3pd) level,[5] but much lower than the computed intensity of $\sim$104 km mol^{-1} derived at the B3LYP/6-31G* level. The gas-phase intensity measurements of the aromatic C–H stretches have been reported for naphthalene ($\sim$96 km mol^{-1}; Cané et al. 1996), anthracene ($\sim$161 km mol^{-1}; Cané et al. 1997), pyrene ($\sim$122 km mol^{-1}; Joblin et al. 1994), and coronene ($\sim$161 km mol^{-1}; Joblin et al. 1994). To our knowledge, no gas-phase IR intensities have been published for phenanthrene and perylene, although the IR absorption spectra of various matrix-isolated PAH species, including phenanthrene and perylene, have been obtained (e.g., see Hudgins & Allamandola 1995a, 1995b, 1997; Hudgins & Sandford 1998a, 1998b; Szczepanski & Vala 1993a, 1993b). Similar to benzene, the experimental intensities are much lower than our calculated results for the aromatic C–H stretches at the B3LYP/6-31G* level, which are respectively $\sim$139, 178, 188, and 257 km mol^{-1} for naphthalene, anthracene, pyrene, and coronene, exceeding their experimental values by $\sim$45%, 11%, 54%, and 60%, respectively.

For toluene, we digitize the NIST experimental spectra and integrate over the range of 3000–3200 cm^{-1} to obtain the intensity of the aromatic C–H stretch (A_{aro}). Similarly, we integrate over the range of 2800–3000 cm^{-1} to obtain the intensity of the aliphatic C–H stretch (A_{ali}). The relative intensity of the methyl (aliphatic) signal to that of the aromatic band is $A_{\mathrm{ali}}/A_{\mathrm{aro}} \approx 0.79$. A similar analysis of the experimental spectrum of Wilmshurst & Bernstein (1957) results in $A_{\mathrm{ali}}/A_{\mathrm{aro}} \approx 0.71$.[6] Our integration of

the NIST spectrum of toluene gives a total intensity of $\sim$97.2 km mol^{-1} for all the C–H stretches (both methyl and aromatic) and is in excellent agreement with the value of $\sim$95 km mol^{-1} calculated by Pavlyuchko et al. (2012) and by Galabov et al. (1992) at the MP2/6-311G(3df,3pd) level. According to our ratio of the measured intensities for the methyl to aromatic regions ($A_{\mathrm{ali}}/A_{\mathrm{aro}} \approx 0.79$), this overall intensity corresponds to intensities of $\sim$42.9 km mol^{-1} for the methyl bands and of $\sim$54.3 km mol^{-1} for the aromatic bands. The intensities computed at the B3LYP/6-31G* level for toluene are $\sim$165.3 km mol^{-1} for the entire region and $\sim$70.4 and $\sim$94.9 km mol^{-1} for the methyl and aromatic sections, respectively. Again, we see that the computed intensities are much higher than the experimental values from the gas-phase measurements.

In the absence of absolute intensity experimental data for naphthalene, anthracene, phenanthrene, perylene, pyrene, and coronene, we are unfortunately not able to compare the experimental intensities of the C–H stretches of these molecules with those computed at the B3LYP/6-31G* level.

3. Scaling Approaches for the Computed Total Intensities of C–H Stretching Modes

As we have seen in Section 2, the IR intensities calculated at the B3LYP/6-31G* level are much higher compared to the experimental results. Using better basis sets in conjunction with the B3LYP method, we found that the IR intensities still differ by a factor of $\sim$30% compared to the experiment results. Pavlyuchko et al. (2012) reported that the IR intensities calculated for benzene and toluene at the level MP2/6-311G (3df,3pd) match the experimental results very well. We have tried to reproduce their data for benzene and toluene by performing both MP2(fc) and MP2(full) computations with the 6-311G(3df,3pd) basis set.[7]

While the MP2(full)/6-311+G(3df,3pd) level data reproduce the measured IR intensities reasonably well, such calculations are far too expensive, especially for large molecules. The MP2(full) computations of the naphthalene systems with the large basis sets including the (3df,3pd) polarization functions each require several days of computer time on eight processors. Considering that the absolute values computed at all of the MP2 levels are better than the respective values computed at the B3LYP levels, one would be inclined to explore scaling approaches of the MP2 data computed with modest basis sets. However, we will show below that scaling approaches that are based on the B3LYP data can be just as successful in spite of the fact that the absolute numbers

---

[4] The intensities for benzene are taken from the 3-term Blackman–Harris entries with a resolution of 0.125 cm^{-1}.

[5] Bertie & Keefe (1994) gave a significantly higher value of $A_{\mathrm{aro}}(\nu_{12}) \approx 73 \pm 9$ km mol^{-1} based on their integration over the range of 3175–2925 cm^{-1}. Note that this region contains some intensity from the (weak) combination bands.

[6] Note that A_{aro} (A_{ali}) is the strength of all the aromatic (aliphatic) C–H stretches, while $A_{3.3}$ ($A_{3.4}$) is the strength of the aromatic (aliphatic) stretch per C–H bond. For toluene, $A_{\mathrm{aro}} = 5A_{3.3}$ and $A_{\mathrm{ali}} = 3A_{3.4}$, therefore we have $A_{3.4}/A_{3.3} = (5/3)A_{\mathrm{ali}}/A_{\mathrm{aro}}$.

[7] The MP2 computations are performed either with the full active space of all core and valence electrons considered in the correlation energy computation, denoted MP2(full), or with the frozen core approximation and the consideration of just the valence electrons in the correlation treatment, denoted MP2(fc). With MP2/6-311G(3df,3pd), Pavlyuchko et al. (2012) calculated the C–H stretch intensities of benzene and toluene to be $\sim$53 km mol^{-1} and $\sim$98 km mol^{-1}, respectively. We have tried both MP2(fc)/6-311G(3df,3pd) and MP2(full)/6-311G(3df,3pd). With MP2(fc)/6-311G(3df,3pd), we obtained $\sim$53.8 km mol^{-1} and $\sim$97.1 km mol^{-1} for benzene and toluene, respectively, while with MP2(full)/6-311G(3df,3pd) these intensities become $\sim$52.4 km mol^{-1} and $\sim$94.7 km mol^{-1}. Although the MP2(fc) results closely match those of Pavlyuchko et al. (2012), the MP2(full) results are closer to the experimental results ($\sim$55 km mol^{-1} for benzene and $\sim$95 km mol^{-1} for toluene). Since MP2(full) considers all the core and valence electrons and thus should be more accurate than MP2(fc), we therefore calculate all other vibrational spectra with MP2(full) in conjunction with the standard basis set 6-31G* and the extended basis sets 6-311+G** and 6-311+G(3df,3pd) for benzene, naphthalene and their mono-methyl derivatives as test cases.

computed at the B3LYP/6-31G* level differ much more from experiment than do the MP2/6-31G* data.

Before we proceed, it is useful to clarify the meaning of scaling approaches. In the most typical approach to scaling, one attempts to reproduce a set of experimental data with a set of data obtained at a level L_i such that $p(\exp) \approx f \cdot p(L_i)$, that is, one scaling factor f is applied to all values in the data set and this scale factor depends on the level, $f = f(L_i)$. This kind of scaling is commonly employed for vibrational frequencies. For intensities, however, we will see that approaches of the type $p(\exp) \approx f \cdot p(L_i) + C(L_i)$ are more successful, that is, there will be a non-zero offset.

Let $ML1$, $ML2$, and $ML3$ respectively represent the MP2(full) computations with the 6-31G*, 6-311+G(d,p), and 6-311+G(3df,3pd) basis sets. Let $BL1$, $BL2$, and $BL3$ respectively represent the B3LYP computations with the 6-31G*, 6-311+G(d,p), and 6-311+G(3df,3pd) basis sets. As can be seen from Figure 2 (top left), the total intensities (A) computed at the MP2 level but with different basis sets [i.e., $A(ML1)$, $A(ML2)$, and $A(ML3)$] are linearly related:

$$A(ML3) \approx 0.7615\, A(ML1), \quad (r^2 \approx 0.9575), \qquad (1a)$$

$$A(ML3) \approx 0.9382\, A(ML1) - 20.4880, \quad (r^2 \approx 0.9949), \qquad (1b)$$

$$A(ML3) \approx 0.8089\, A(ML2), \quad (r^2 \approx 0.9984), \qquad (1c)$$

where r^2 is the linear correlation coefficient. While Equation 1(c) describes an excellent linear correlation between the intensities computed with the $ML3$ method and those with the $ML2$ method without any need for an offset, the analogous Equation 1(a) is less successful and is an excellent linear correlation between $A(ML3)$ and $A(ML1)$ only is achieved when a non-zero offset is allowed in Equation 1(b). The analogous relations also hold at the B3LYP level (Equation 2) and they are shown in Figure 2 (top right), where $A(BL1)$, $A(BL2)$, and $A(BL3)$ are respectively the intensities computed at the $BL1$, $BL2$, and $BL3$ levels.

$$A(BL3) \approx 0.7306\, A(BL1), \quad (r^2 \approx 0.9610), \qquad (2a)$$

$$A(BL3) \approx 0.8838\, A(BL1) - 26.1670, \quad (r^2 \approx 0.9924), \qquad (2b)$$

$$A(BL3) \approx 0.8089\, A(BL2), \quad (r^2 \approx 0.9984), \qquad (2c)$$

$$A(BL3) \approx 0.8395\, A(BL2) - 3.3861, \quad (r^2 \approx 0.9998). \qquad (2d)$$

Also shown in Figure 2 (bottom left) are the nearly linear relations between the IR intensities computed at the B3LYP and MP2(full) levels with a common basis set. The data are very well described by linear regression and there is no need for a non-zero offset in any of the following equations (see Equations 3(a)–(c)). It is remarkable that these slopes are rather similar for the various basis sets.

$$A(ML1) \approx 0.6769\, A(BL1), \quad (r^2 \approx 0.9971), \qquad (3a)$$

$$A(ML2) \approx 0.7877\, A(BL2), \quad (r^2 \approx 0.9966), \qquad (3b)$$

$$A(ML3) \approx 0.7056\, A(BL3), \quad (r^2 \approx 0.9949). \qquad (3c)$$

In light of these linear correlations, it is clear that there must be a strong linear correlation between the lowest DFT level, our standard level B3LYP/6-31G* (i.e., $BL1$), and the best MP2 level, the level MP2(full)/6-311+G(3df,3pd) (i.e., $ML3$).

Equations 1(a) and 3(a) suggest a correlation coefficient of $\approx 0.7615 \times 0.6769 \approx 0.5154$ and the actual correlation coefficient of Equation 4(a) is ~ 0.5152 and it is essentially the same (see Figure 2, bottom right). Considering the need for non-zero offset in Equation 1(b), we also explore Equation 4(b) and achieve an excellent linear correlation:

$$A(ML3) \approx 0.5152\, A(BL1), \quad (r^2 \approx 0.9428), \qquad (4a)$$

$$A(ML3) \approx 0.6655\, A(BL1) - 25.6770, \quad (r^2 \approx 0.9964). \qquad (4b)$$

This shows that, by applying this scaling relation (Equation 4(b)), we just need to perform computations at an inexpensive level (e.g., B3LYP/6-31G*) and we are still able to obtain intensities as accurate as those computed at far more advanced levels [e.g., MP2/6-311+G(3df,3pd)].

4. Astrophysical Implications

As shown in Yang et al. (2013), the aromatic C–H stretch band strength does not vary significantly for different molecules. It has an average value (per aromatic C–H bond) of $\langle A_{3.3} \rangle \approx 14.03$ km mol^{-1}, with a standard deviation of $\sigma(A_{3.3}) \approx 0.89$ km mol^{-1}. On the other hand, the aliphatic C–H stretch band strength is more dependent on the nature of the molecule and also on the specific isomer. The average band strength (per aliphatic C–H bond) is $\langle A_{3.4} \rangle \approx 23.68$ km mol^{-1}, and the standard deviation is $\sigma(A_{3.4}) \approx 2.48$ km mol^{-1}. All of these values are calculated for neutral PAHs at the B3LYP/ 6-311+G** (i.e., $BL2$) level. As discussed in Section 3, these values need to be scaled. By taking MP2(full)/6-311+G (3df,3pd) (i.e., $ML3$) to be the level that gives the most reliable band strength, the intensities need to be scaled with two formulae: Equations 1(c) and 3(b). Thus, we derive for neutral PAHs $\langle A_{3.3} \rangle \approx 14.03 \times 0.7877 \times 0.8089 \approx 8.94$ km mol^{-1} (i.e., $\sim 1.49 \times 10^{-18}$ cm per C–H bond), $\langle A_{3.4} \rangle \approx 23.68 \times 0.7877 \times 0.8089 \approx 15.09$ km mol^{-1} (i.e., $\sim 2.50 \times 10^{-18}$ cm per C–H bond), and $\langle A_{3.4} \rangle / \langle A_{3.3} \rangle \approx 1.69$. Similarly, we obtain for PAH cations $\langle A_{3.3} \rangle \approx 0.92$ km mol^{-1}, $\langle A_{3.4} \rangle \approx 3.20$ km mol^{-1}, and $\langle A_{3.4} \rangle / \langle A_{3.3} \rangle \approx 3.48$. We note that, although these results were derived from the mono-methyl derivatives of small PAH molecules, it has been shown in Yang et al. (2016b) that the $A_{3.4}/A_{3.3}$ ratios determined from the PAH molecules attached with a wide range of sidegroups (including ethyl, propyl, and butyl) as well as dimethyl-substituted pyrene are close to those of mono-methyl PAHs.

In addition to the 3.4 μm C–H stretch, PAHs with aliphatic sidegroups also have two aliphatic C–H deformation bands at 6.85 and 7.25 μm. Yang et al. (2016a) have derived $A_{6.85}$ and $A_{7.25}$, the intrinsic oscillator strengths of the 6.85 and 7.25 μm aliphatic C–H deformation bands for both neutral and ionized methyl-substituted PAHs. They obtained lower limits of $A_{6.85}/A_{6.2} \approx 5.0$ and $A_{7.25}/A_{6.2} \approx 0.5$ for neutrals, $A_{6.85}/A_{6.2} \approx 0.5$ and $A_{7.25}/A_{6.2} \approx 0.25$ for cations, where $A_{6.2}$ is the intrinsic oscillator strength of the 6.2 μm aromatic C–C stretch.

With $A_{3.4}/A_{3.3}$, $A_{6.85}/A_{6.2}$, and $A_{7.25}/A_{6.2}$ derived for both neutral and ionized PAHs, we now calculate the emission spectra of methyl PAHs excited by starlight and the corresponding model band ratios $I_{3.4}/I_{3.3}$. Consider a PAH molecule containing $N_{C,aro}$ aromatic C atoms and $N_{C,ali}$
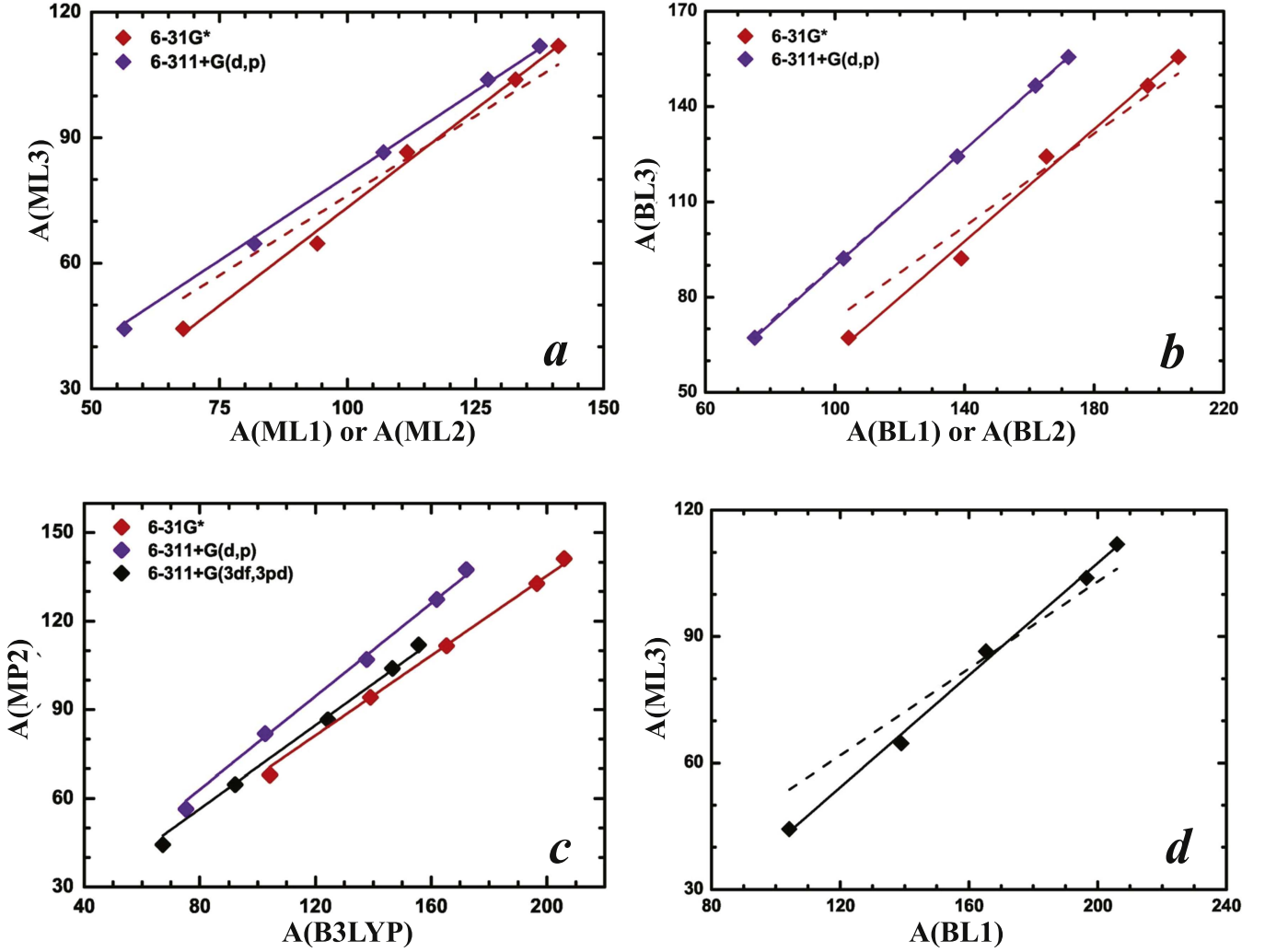
Figure 2. Level dependency of the total C–H stretch intensities (methyl plus aromatic) for benzene and naphthalene and for their methyl derivatives toluene and methylnaphthalene. Top left (a): intensities calculated at MP2 with small basis sets (i.e., 6-31G* (i.e., *ML1*), 6-311+G(d,p) (i.e., *ML2*)) vs. those with a large basis set [6-311+G(3df,3pd) (i.e., *ML3*)]. The dashed red line plots Equation 1(a), the solid red line plots Equation 1(b), and the solid blue line plots Equation 1(c). Top right (b): same as (a) but at B3LYP. The dashed red line plots Equation 2(a), the solid red line plots Equation 2(b), the dashed blue line plots Equation 2(c), and the solid blue line plots Equation 2(d). Bottom left (c): intensities calculated at B3LYP vs. MP2 with the same basis set. The solid red line plots Equation 3(a), the solid blue line plots Equation 3(b), and the solid black line plots Equation 3(c). Bottom right (d): intensities calculated at B3LYP/6-31G* (i.e., *BL1*) vs. MP2/6-311+G(3df,3pd) (i.e., *ML3*). The dashed black line plots Equation 4(a), and the solid black line plots Equation 4(b)

aliphatic C atoms (i.e., $N_{C,ali}$ methyl sidegroups). We approximate their absorption cross-sections by adding three Drude functions to those of PAHs of $N_{C,aro}$ aromatic C atoms, with these Drude functions respectively representing the 3.4 μm aliphatic C–H stretch, and the 6.85 and 7.25 μm aliphatic C–H deformations:

$$C_{abs}(N_C, \lambda) = C_{abs}^{PAH}(N_{C,aro}, \lambda), \tag{5}$$

$$+ N_{C,ali} \frac{2}{\pi} \frac{\gamma_{3.4} \lambda_{3.4} \sigma_{int,3.3} (A_{3.4}/A_{3.3})}{(\lambda/\lambda_{3.4} - \lambda_{3.4}/\lambda)^2 + \gamma_{3.4}^2}, \tag{6}$$

$$+ N_{C,ali} \frac{2}{\pi} \frac{\gamma_{6.85} \lambda_{6.85} \sigma_{int,6.2} (A_{6.85}/A_{6.2})}{(\lambda/\lambda_{6.85} - \lambda_{6.85}/\lambda)^2 + \gamma_{6.85}^2}, \tag{7}$$

$$+ N_{C,ali} \frac{2}{\pi} \frac{\gamma_{7.25} \lambda_{7.25} \sigma_{int,6.2} (A_{7.25}/A_{6.2})}{(\lambda/\lambda_{7.25} - \lambda_{7.25}/\lambda)^2 + \gamma_{7.25}^2}, \tag{8}$$

where $N_C = N_{C,aro} + N_{C,ali}$; $\lambda_{3.4} = 3.4$ μm, $\lambda_{6.85} = 6.85$ μm, and $\lambda_{7.25} = 7.25$ μm are respectively the peak wavelengths of

the 3.4, 6.85, and 7.25 μm features; $\gamma_{3.4} \lambda_{3.4} = 0.03$ μm, $\gamma_{6.85} \lambda_{6.85} = 0.2$ μm, and $\gamma_{7.25} \lambda_{7.25} = 0.2$ μm are respectively the mean FWHMs of the astronomical 3.4, 6.85, and 7.25 μm features (Yang et al. 2013, 2016a),[8] and $\sigma_{int,3.3}$ and $\sigma_{int,6.2}$ are respectively the integrated strengths per (aromatic) C atom of the 3.3 μm aromatic C–H stretch and 6.2 μm aromatic C–C stretch (see Draine & Li 2007).

Due to their small size (and therefore small heat capacity), PAHs are heated sporadically by single-starlight photons. Unless exposed to an extremely intense radiation field, PAHs will undergo strong temperature fluctuations and will not attain an equilibrium temperature (see Li 2004). We take the "thermal-discrete" technique developed by Draine & Li (2001) to calculate the temperature probability distribution functions and the resulting emission spectra of methyl PAHs.

---

[8] As defined by Draine & Li (2007), $\gamma_{3.4}$, $\gamma_{6.85}$, and $\gamma_{7.25}$ are dimensionless parameters.
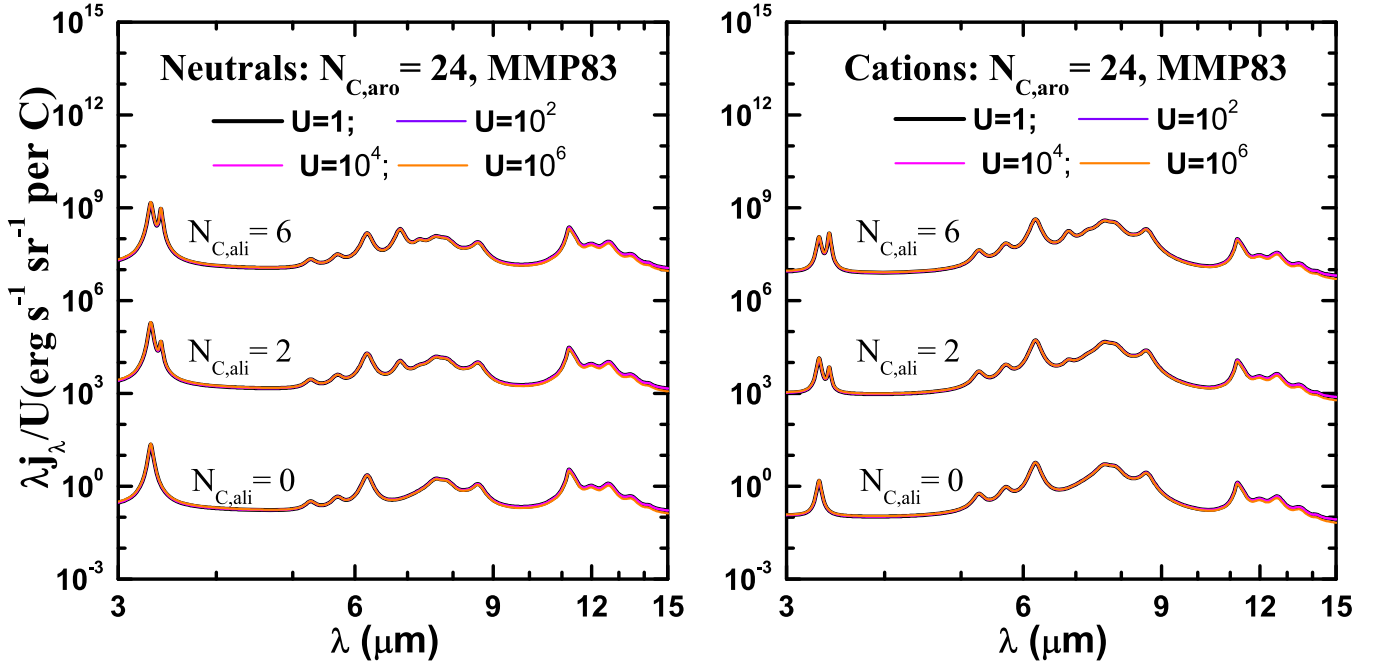
Figure 3. IR emission spectra of neutral (left panel) and ionized (right panel) methyl PAHs of $N_{C,ali} = 0, 2, 6$ aliphatic C atoms and $N_{C,aro} = 24$ aromatic C atoms illuminated by the MMP83 ISRF of various intensities ($U = 1$: black lines; $U = 100$: purple lines; $U = 10^4$: magenta lines; and $U = 10^6$: red lines). The 3.4 and 6.85 μm aliphatic C–H features are clearly seen in the spectra of methyl PAHs with $N_{C,ali} = 2, 6$, while the 7.25 μm aliphatic C–H feature is less prominent. For clarity, their spectra are vertically shifted.
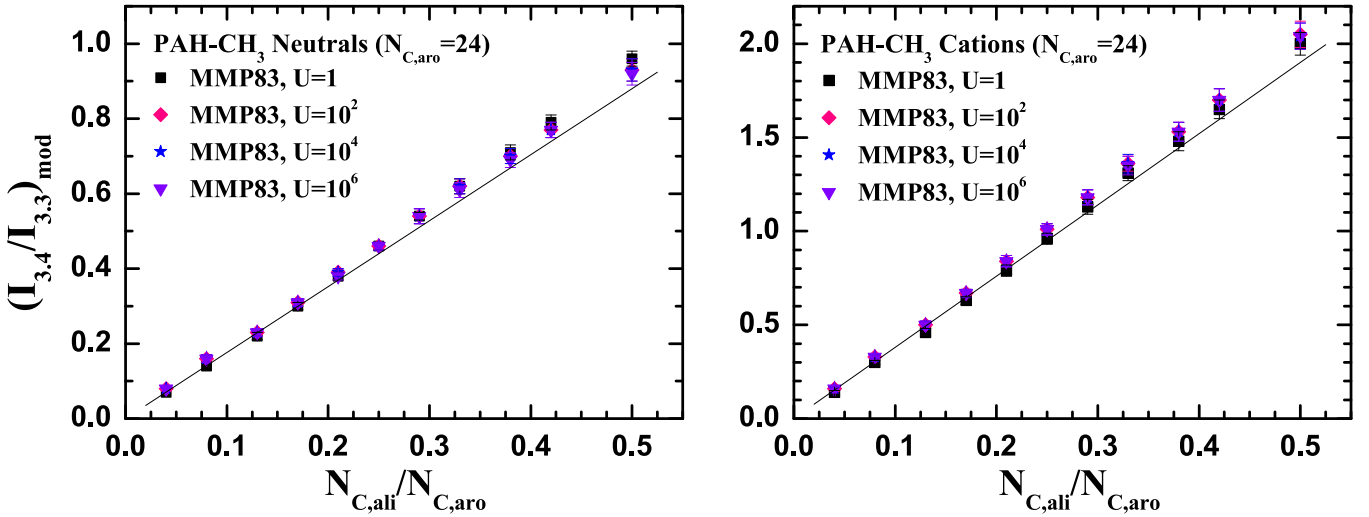
Figure 4. Model-calculated intensity ratios $(I_{3.4}/I_{3.3})_{mod}$ as a function of the aliphatic fraction $N_{C,ali}/N_{C,aro}$ for neutral methyl PAHs of $N_{C,aro} = 24$ (left panel) and their cations (right panel). The molecules and their cations are illuminated by the MMP83 ISRF with the starlight intensity enhanced by a factor of U ($U = 1$: black squares; $U = 100$: red diamonds; $U = 10^4$: blue stars; $U = 10^6$: purple triangles). The solid black line plots $(I_{3.4}/I_{3.3})_{mod} = 1.76 \times (N_{C,ali}/N_{C,aro})$ for neutrals and $(I_{3.4}/I_{3.3})_{mod} = 3.80 \times (N_{C,ali}/N_{C,aro})$ for cations.

Let dP be the probability that the temperature of the molecule will be in $[T, T + dT]$. The emissivity of this molecule (of N_C C atoms) becomes

$$j_\lambda(N_C) = \int C_{abs}(N_C, \lambda) 4\pi B_\lambda(T) \frac{dP}{dT} dT, \qquad (9)$$

where $B_\lambda(T)$ is the Planck function at wavelength λ and temperature T. As shown in Figures 6 and 7 of Draine & Li (2007), the 3.3 μm interstellar UIE emitters are in the size range of $N_C \sim 20$–30 C atoms. For illustrative purposes, we therefore consider $N_{C,aro} = 24$ (like coronene). For a coronene-like

molecule, up to 12 methyl sidegroups can be attached to it. We thus consider methyl PAHs of $N_{C,ali} = 0, 1, 2, ..., 12$ aliphatic C atoms. For all molecules, we fix $N_{C,aro} = 24$. In Figure 3 we show the IR emission spectra of both neutral and ionized methyl PAHs of $N_{C,ali} = 0, 2, 6$ illuminated by the solar neighborhood interstellar radiation field (ISRF) of Mathis et al. (1983; MMP83). Figure 3 shows that, the 3.4 and 6.85 μm features are clearly visible in the IR emission spectra for $N_{C,ali} = 2$, while the 7.25 μm feature remains hardly noticeable even for $N_{C,ali} = 6$. This is because the intrinsic strength of the 7.25 μm feature is weaker than that of the 6.85 μm feature by a
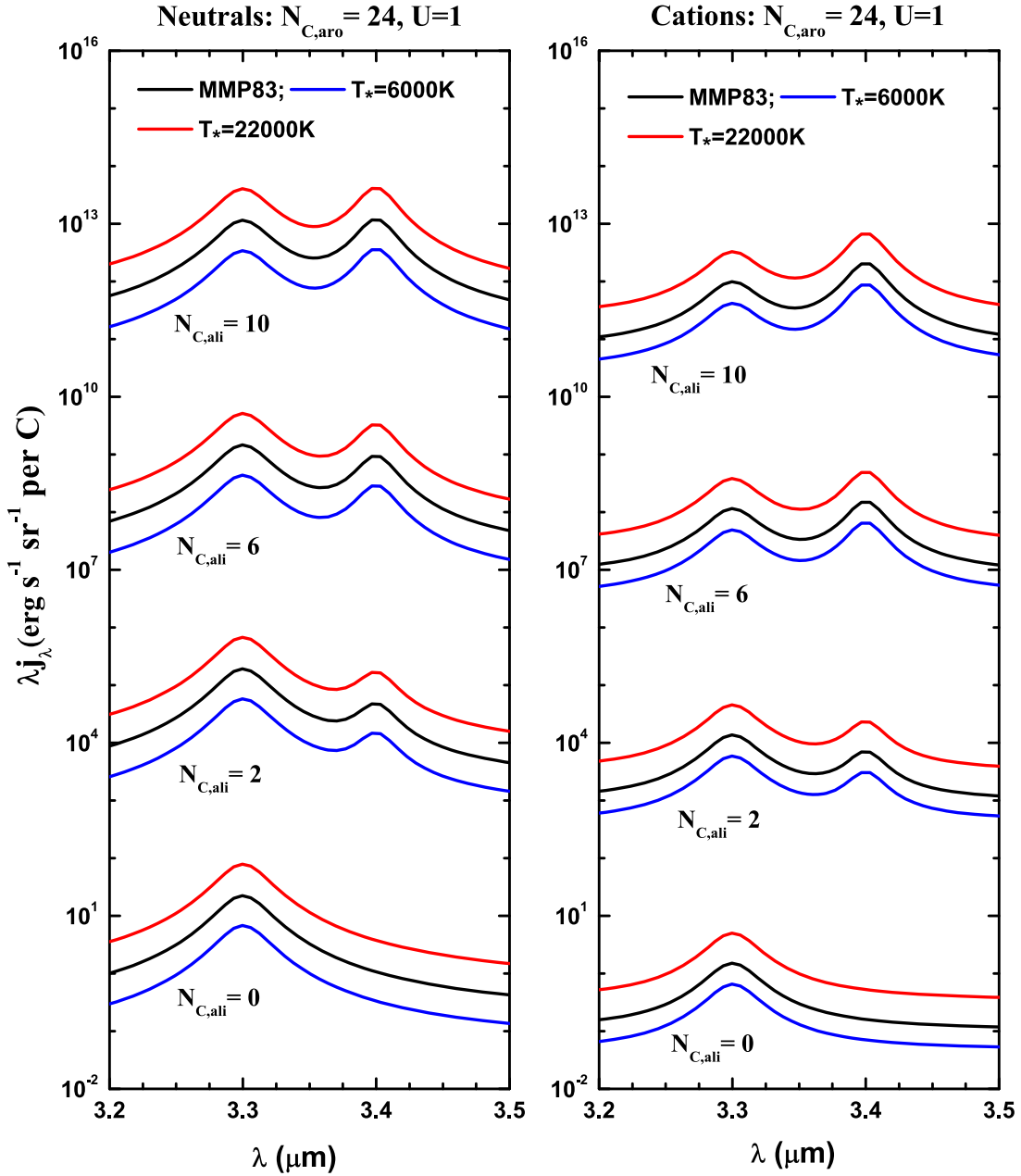
Figure 5. IR emission spectra of neutral (left panel) and ionized (right panel) methyl PAHs of $N_{C,ali} = 0$, 2, 6, 10 aliphatic C atoms and $N_{C,aro} = 24$ aromatic C atoms illuminated by a solar-type star of $T_\star = 6000$ K (blue lines), a B1.5V star of $T_\star = 22,000$ K (red lines), and the MMP83 ISRF (black lines). The starlight intensities are all set to be $U = 1$. For clarity, the spectra for methyl PAHs with $N_{C,ali} = 2$, 6, 10 are vertically shifted.

factor of ~8 for neutral methyl PAHs and by a factor of ~3 for their cations (Yang et al. 2016a). In the following discussions, we will focus on the 3.3 and 3.4 μm features since the molecules considered here are too small to be the dominant UIE emitters at ~6–8 μm (see Figures 6 and 7 of Draine & Li 2007).

We have also explored the effects of starlight intensities on the IR emission spectra of methyl PAHs by increasing the MMP ISRF by a factor of U. As shown in Figure 3, the resulting IR emission spectra for $U = 1$, 100, 10^4, 10^6, after being scaled by U, are essentially identical. This is not unexpected. The single-photon heating nature of these molecules assures that their IR emission spectra (scaled by the starlight intensity) remain the same for different starlight

intensities. Single-photon heating implies that the shape of the high-T end of the temperature probability distribution function dP/dT for a methyl PAH is the same for different levels of starlight intensity, and what only matters is the mean photon energy (which determines what peak temperature a molecule will reach, upon absorption of such a photon; see Draine & Li 2001; Li 2004).

For a given $N_{C,ali}$, we derive $(I_{3.4}/I_{3.3})_{mod}$, the model intensity ratio of the 3.4 μm band to the 3.3 μm band, from

$$\left(\frac{I_{3.4}}{I_{3.3}}\right)_{mod} = \frac{\int_{3.4} \Delta j_\lambda(N_C)d\lambda}{\int_{3.3} \Delta j_\lambda(N_C)d\lambda}, \qquad (10)$$
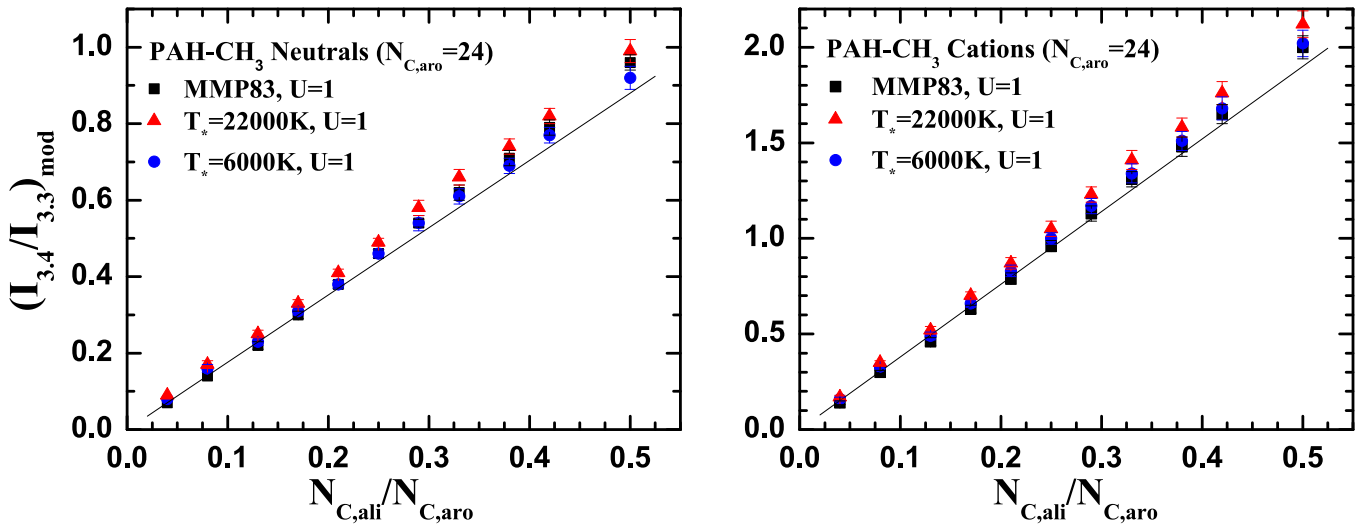
Figure 6. Model-calculated intensity ratios $(I_{3.4}/I_{3.3})_{mod}$ as a function of the aliphatic fraction $N_{C,ali}/N_{C,aro}$ for neutral methyl PAHs of $N_{C,aro} = 24$ (left panel) and their cations (right panel). The molecules and their cations are illuminated by a solar-type star of $T_\star = 6000$ K (blue circles), a B1.5V star of $T_\star = 22,000$ K (red triangles), and the MMP83 ISRF (black squares). The starlight intensities are all set to be $U = 1$. The solid black line plots $(I_{3.4}/I_{3.3})_{mod} = 1.76 \times (N_{C,ali}/N_{C,aro})$ for neutrals and $(I_{3.4}/I_{3.3})_{mod} = 3.80 \times (N_{C,ali}/N_{C,aro})$ for cations.

where $\int_{3.3} \Delta j_\lambda (N_C) d\lambda$ and $\int_{3.4} \Delta j_\lambda (N_C) d\lambda$ are respectively the feature-integrated excess emission of the 3.3 and 3.4 μm features of the methyl PAH molecule. In Figure 4 we show the model intensity ratios $(I_{3.4}/I_{3.3})_{mod}$ as a function of $N_{C,ali}/N_{C,aro}$ for neutral and ionized methyl PAHs. It is encouraging to see in Figure 4 that, with $N_{C,ali}/N_{C,aro} = 0.5$, $(I_{3.4}/I_{3.3})_{mod}$ reaches ~0.9 for neutrals and ~2.0 for cations, demonstrating that the unusually high $(I_{3.4}/I_{3.3})_{obs}$ ratios observed in some protoplanetary nebulae (e.g., IRAS 04296+3429 with $(I_{3.4}/I_{3.3})_{obs} \approx 1.54$) can be accounted for by a mixture of neutral and ionized methyl PAHs, with a reasonable fraction of C atoms in methyl sidegroups. In Figure 4 we also compare the model band ratios with the ratios computed from the simple relation $(I_{3.4}/I_{3.3})'_{mod} = 1.76 \times (N_{C,ali}/N_{C,aro})$ for neutrals or $(I_{3.4}/I_{3.3})'_{mod} = 3.80 \times (N_{C,ali}/N_{C,aro})$ for cations. Figure 4 shows that this simple, straightforward relation does an excellent job of accurately predicting $(I_{3.4}/I_{3.3})_{mod}$. This is nice because in future studies one can simply use this convenient relation to determine the aliphatic fraction $N_{C,ali}/N_{C,aro}$ of the UIE carrier from the observed band ratio $(I_{3.4}/I_{3.3})_{obs}$: $N_{C,ali}/N_{C,aro} \approx 0.57 \times (I_{3.4}/I_{3.3})_{obs}$ for neutrals and $N_{C,ali}/N_{C,aro} \approx 0.26 \times (I_{3.4}/I_{3.3})_{obs}$ for cations. There is no need to compute the temperature probability distribution functions and the IR emission spectra of methyl PAHs as long as one is only interested in the aliphatic fraction of the UIE carrier.

So far, we have only considered methyl PAHs excited by MMP83-type starlight. To examine whether and how the spectral shape of the exciting starlight affects the model IR emission spectra and the band ratios $(I_{3.4}/I_{3.3})_{mod}$, we consider methyl PAHs of $N_{C,ali} = 0, 1, 2, ... 12$ aliphatic C atoms and $N_{C,ali} = 24$ aromatic C atoms excited by stars with an effective temperature of $T_\star = 6000$ K like our Sun and by stars of $T_\star = 22,000$ K like the B1.5V star HD 37903, which illuminates the reflection nebula NGC 2023. We fix the starlight intensity in the 912 Å–1 μm wavelength range to be that of the MMP83 ISRF (i.e., $U = 1$):

$$\int_{1\mu m}^{912\,\text{Å}} 4\pi J_\star(\lambda, T_\star) d\lambda = \int_{1\mu m}^{912\,\text{Å}} 4\pi J_{ISRF}(\lambda) d\lambda, \qquad (11)$$

where $J_\star(\lambda, T_\star)$ is the intensity of starlight approximated by the Kurucz model atmospheric spectrum, and $J_{ISRF}(\lambda)$ is the MMP83 ISRF starlight intensity. As shown in Figure 5, for a given $N_{C,ali}/N_{C,aro}$, the $T_\star = 6000$ K model results in a lower emissivity level than that of the MMP83 ISRF model. In contrast, the $T_\star = 22,000$ K model results in a higher emissivity level than that of the MMP83 ISRF model. This is because, exposed to a *softer* radiation field, PAHs absorb individual photons with a *lower* mean energy than that of a *harder* radiation field and therefore emit less (because they absorb less). Nevertheless, the emission spectral profiles are very similar to each other. This is also illustrated in Figure 6, which shows that the model band ratios $(I_{3.4}/I_{3.3})_{mod}$ differ very little for methyl PAHs excited by starlight of different spectral shapes.

So far, we have confined ourselves to coronene-like PAHs with $N_{C,aro} = 24$. To examine the effects of the PAH size on the model IR emission spectra and the band ratios $(I_{3.4}/I_{3.3})_{mod}$, we consider methyl PAHs of $N_{C,aro} = 20$ aromatic C atoms (like perylene) and $N_{C,ali} = 0, 1, 2, ... 12$ aliphatic C atoms, as well as methyl PAHs of $N_{C,aro} = 32$ aromatic C atoms (like ovalene) and $N_{C,ali} = 0, 1, 2, ... 14$ aliphatic C atoms.[9] As shown in Figures 7 and 8, neither the IR emission spectra in the C–H stretch region nor the band ratios $(I_{3.4}/I_{3.3})_{mod}$ appreciably differ from each other.

Finally, we compare in Figure 9 the band ratios $(I_{3.4}/I_{3.3})_{obs}$ observed in the eight representative astrophysical environments shown in Figure 1 with those calculated from methyl PAHs. It is seen that the observed band ratios $(I_{3.4}/I_{3.3})_{obs}$ of all sources

---

[9] We note that it is not necessary to consider larger PAHs since the 3.3 μm C–H feature is predominantly emitted by small neutral PAHs of ~20–30 C atoms (see Figures 6, 7 of Draine & Li 2007).
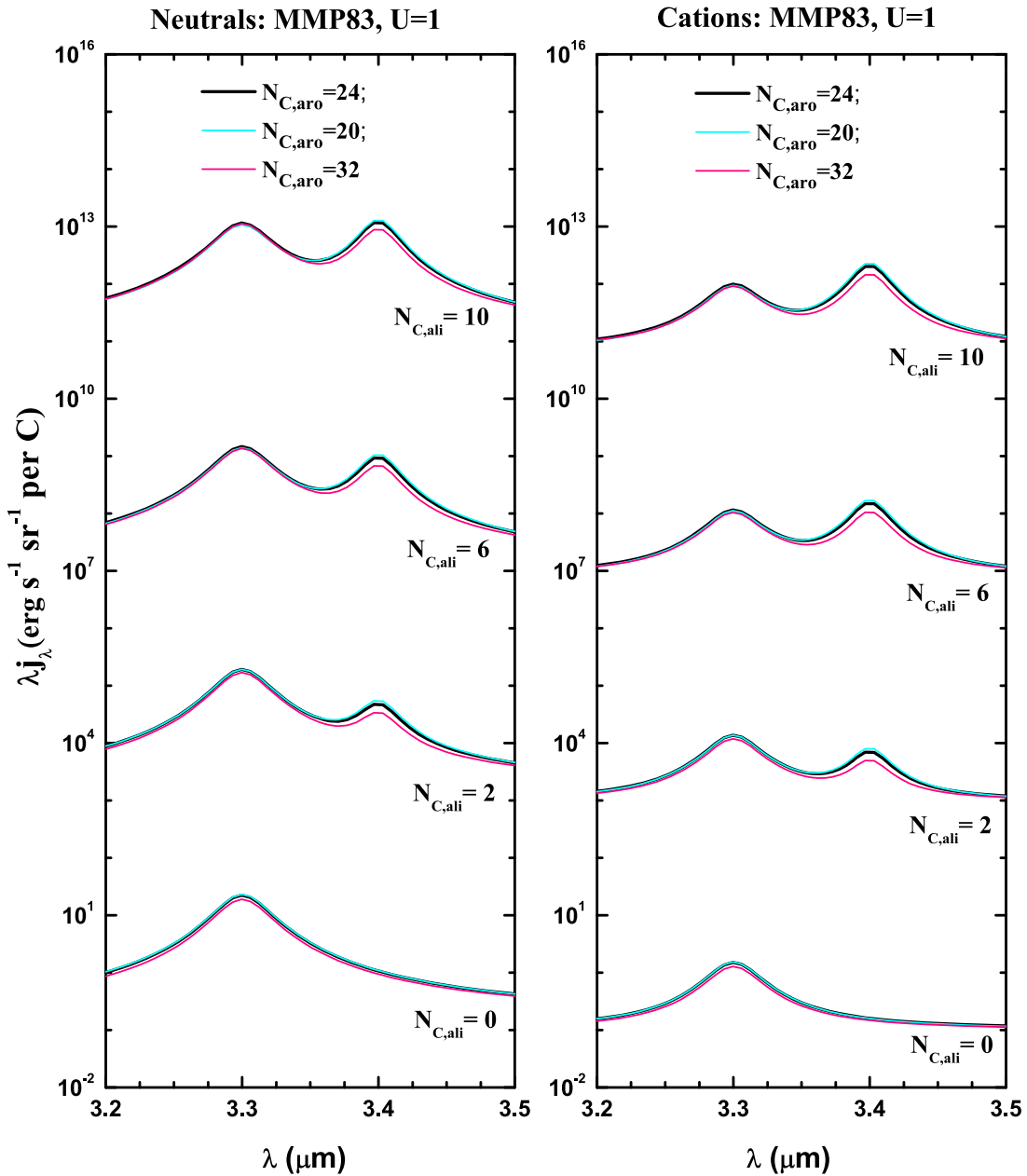
Figure 7. IR emission spectra of neutral (left panel) and ionized (right panel) methyl PAHs of $N_{C,ali} = 0$, 2, 6, 10 aliphatic C atoms and $N_{C,aro} = 20$ (cyan lines), $N_{C,aro} = 24$ (black lines), or $N_{C,aro} = 32$ (red lines) illuminated by the MMP83 ISRF ($U = 1$). For clarity, the spectra for methyl PAHs with $N_{C,ali} = 2$, 6, 10 are vertically shifted.

except the protoplanetary nebula IRAS 04296+3429 all fall below the model $(I_{3.4}/I_{3.3})_{mod}$ curve of neutral PAHs with $N_{C,aro} = 24$ and $N_{C,ali}/N_{C,aro} \lesssim 0.5$. For IRAS 04296+3429, the unusually high ratio of $(I_{3.4}/I_{3.3})_{obs} \approx 1.54$ falls below the model $(I_{3.4}/I_{3.3})_{mod}$ curve of PAH cations. This demonstrates that a mixture of neutral and ionized methyl PAHs are capable of accounting for all the observed band ratios, including those of protoplanetary nebulae, some of which exhibit an extremely strong 3.4 μm feature.

5. Summary

We have presented an intensity scaling scheme for scaling the band strengths of the C–H stretching features of PAHs with a methyl side chain computed with B3LYP, which is less

accurate and computationally less demanding. Such an intensity scaling approach allows us to obtain accurate band strengths, as accurate as those computed with MP2 in conjunction with large basis sets, which is known to be more accurate than B3LYP but computationally very expensive. It is found that the band intensities calculated with B3LYP/6-31G* for a number of molecules are much higher than their gas-phase experimental values. Using better basis sets in conjunction with the B3LYP method, the computed intensities are still considerably higher (by ~30%) compared to their experimental results. The MP2 method with a basis set of 6-311+G(3df,3pd) reproduces the measured intensities reasonably well. However, such calculations are far too expensive, especially for large molecules. It is shown that intensity scaling approaches that are based on the B3LYP data can be just as successful.
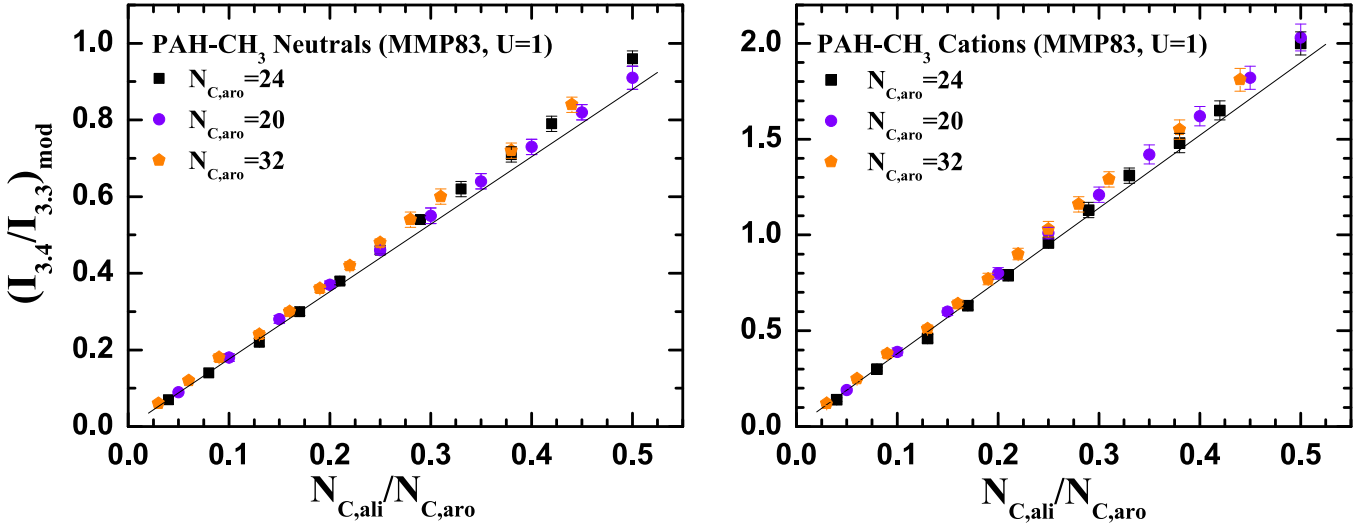
Figure 8. Model-calculated intensity ratios $(I_{3.4}/I_{3.3})_{mod}$ as a function of the aliphatic fraction $N_{C,ali}/N_{C,aro}$ for neutral methyl PAHs (left panel) of $N_{C,aro} = 20$ (purple circles), $N_{C,aro} = 24$ (black squares), and $N_{C,aro} = 32$ (orange pentagons), and their cations (right panel). The molecules and their cations are illuminated by the MMP83 ISRF ($U = 1$). The solid black line plots $(I_{3.4}/I_{3.3})_{mod} = 1.76 \times (N_{C,ali}/N_{C,aro})$ for neutrals and $(I_{3.4}/I_{3.3})_{mod} = 3.80 \times (N_{C,ali}/N_{C,aro})$ for cations.
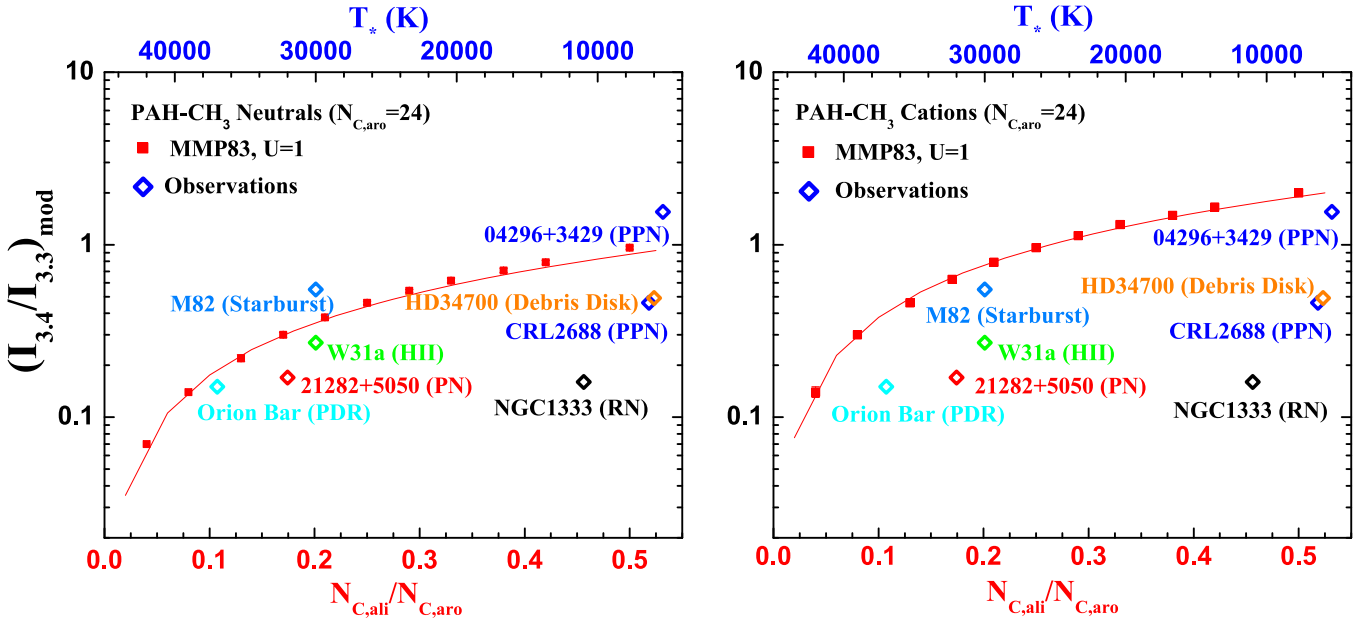

Figure 9. Comparison of the band ratios $(I_{3.4}/I_{3.3})_{obs}$ observed in the eight representative astrophysical environments shown in Figure 1 with those calculated from neutral (left panel) and ionized (right panel) methyl PAHs illuminated by the MMP83 ISRF ($U = 1$). These molecules have $N_{C,aro} = 24$ aromatic C atoms and a wide range of aliphatic fractions $N_{C,ali}/N_{C,aro}$. The upper horizontal axis plots the effective temperatures of the stars illuminating the observed sources.

We have also calculated the model spectra of methylated PAHs and their cations of different sizes and various numbers of methyl sidegroups, excited by the starlight of different spectral shapes and intensities. We find that the ratio of the model intensity of the 3.4 μm feature to that of the 3.3 μm feature is insensitive to the PAH size and the spectral shape and intensity of the exciting starlight. We have derived a simple, convenient, and straightforward relation for determining the aliphatic fraction $N_{C,ali}/N_{C,aro}$ of the 3.3 μm band carriers from the observed band ratios $(I_{3.4}/I_{3.3})_{obs}$: $N_{C,ali}/N_{C,aro} \approx 0.57 \times (I_{3.4}/I_{3.3})_{obs}$ for neutrals and $N_{C,ali}/N_{C,aro} \approx 0.26 \times (I_{3.4}/I_{3.3})_{obs}$ for cations.

Appendix
Rationale for A Non-zero Offset in the Intensity Scaling Relation

We show here that the non-zero offset in the intensity scaling relation (see Section 3) comes from the fact that the intensities of methyl (aliphatic) and aromatic C–H stretches do not scale alike (i.e., $f_{ali} \neq f_{aro}$). Equations 12(a) and (b) show the total intensities of the C–H stretching regions as a function of the

numbers of methyl ($n_{3.4}$) and aromatic ($n_{3.3}$) C–H bonds and the average IR intensities of a methyl ($A_{3.4}$) or of an aromatic ($A_{3.3}$) C–H stretching bond for two theoretical levels L_i and L_j:

$$A(L_i) = n_{3.4}\, A_{3.4}(L_i) + n_{3.3}\, A_{3.3}(L_i), \tag{12a}$$

$$A(L_j) = n_{3.4}\, A_{3.4}(L_j) + n_{3.3}\, A_{3.3}(L_j), \tag{12b}$$

where $A_{3.4}(L_i)$ and $A_{3.3}(L_i)$ are respectively the strengths of one aliphatic or one aromatic C–H bond computed at the L_i level, and $A_{3.4}(L_j)$ and $A_{3.3}(L_j)$ are the same parameters but computed at the L_j level.

Assuming that the intensities of the methyl (aliphatic) and aromatic C–H stretches scale with factors f_{ali} and f_{aro}, respectively, one can express the total intensity at level L_j as a function of the average IR intensities of a methyl (aliphatic) or of an aromatic C–H stretching bond at theoretical levels L_i (i.e., $A_{3.4}(L_i)$ and $A_{3.3}(L_i)$; see Equation 13(a)). By addition and subtraction of the term $f_{\mathrm{aro}}\, n_{3.4}\, A_{3.4}(L_i)$, it is possible to rewrite Equation 13(a) such that $A(L_j)$ is expressed as a function of $A(L_i)$ and $A_{3.4}(L_i)$ (see Equation 13(d)). Using instead the analogous term $f_{\mathrm{ali}}\, n_{3.3}\, A_{3.3}(L_i)$ gives $A(L_j)$ as a function of $A(L_i)$ and $A_{3.3}(L_i)$ (see Equation 14(d)).

$$A(L_j) = f_{\mathrm{ali}}\, n_{3.4}\, A_{3.4}(L_i) + f_{\mathrm{aro}}\, n_{3.3}\, A_{3.3}(L_i), \tag{13a}$$

$$= f_{\mathrm{ali}}\, n_{3.4}\, A_{3.4}(L_i) + f_{\mathrm{aro}}\, n_{3.3}\, A_{3.3}(L_i) + f_{\mathrm{aro}}\, n_{3.4}\, A_{3.4}(L_i) - f_{\mathrm{aro}}\, n_{3.4}\, A_{3.4}(L_i), \tag{13b}$$

$$= f_{\mathrm{aro}}\, [n_{3.4}\, A_{3.4}(L_i) + n_{3.3}\, A_{3.3}(L_i)] + f_{\mathrm{ali}}\, n_{3.4}\, A_{3.4}(L_i) - f_{\mathrm{aro}}\, n_{3.4}\, A_{3.4}(L_i), \tag{13c}$$

$$= f_{\mathrm{aro}}\, A(L_i) + \underline{(f_{\mathrm{ali}} - f_{\mathrm{aro}})n_{3.4}\, A_{3.4}(L_i)}, \tag{13d}$$

or

$$A(L_j) = f_{\mathrm{ali}}\, n_{3.4}\, A_{3.4}(L_i) + f_{\mathrm{aro}}\, n_{3.3}\, A_{3.3}(L_i), \tag{14a}$$

$$= f_{\mathrm{ali}}\, n_{3.4}\, A_{3.4}(L_i) + f_{\mathrm{aro}}\, n_{3.3}\, A_{3.3}(L_i) + f_{\mathrm{ali}}\, n_{3.3}\, A_{3.3}(L_i) - f_{\mathrm{ali}}\, n_{3.3}\, A_{3.3}(L_i), \tag{14b}$$

$$= f_{\mathrm{aro}}\, [n_{3.4}\, A_{3.4}(L_i) + n_{3.3}\, A_{3.3}(L_i)] + f_{\mathrm{aro}}\, n_{3.3}\, A_{3.3}(L_i) - f_{\mathrm{ali}}\, n_{3.3}\, A_{3.3}(L_i), \tag{14c}$$

$$= f_{\mathrm{ali}}\, A(L_i) + \underline{(f_{\mathrm{aro}} - f_{\mathrm{ali}})n_{3.3}\, A_{3.3}(L_i)}, \tag{14d}$$

where the underlined terms in Equations 13(d) and 14(d) are responsible for the offset in the correlations between the total intensities at levels L_i and L_j, and these offsets vanish only when $f_{\mathrm{aro}} = f_{\mathrm{ali}}$. This condition never holds, and in addition, it also is not trivial to determine at what level f_{aro} and f_{ali} converge. We have extensively studied the basis set effects at the B3LYP level for toluene and the three isomers of methylpyrene (see Yang et al. 2013). There is a very large basis set dependency in that $A_{3.3}$ is greatly reduced with the improvements of the basis set. The typical $A_{3.3}$ value at the B3LYP/6-31G* level is $\sim$18–20 km mol^{-1} and this value drops to $\sim$12.5–13.3 km mol^{-1} at the highest level 6-311++G (3df,3pd), i.e., a scaling factor of $f_{\mathrm{aro}} \approx 0.7$. In contrast, the basis set dependency of $A_{3.4}$ is less than that of $A_{3.3}$. A typical $A_{3.4}$ value at the B3LYP/6-31G* level is $\sim$23–27 km mol^{-1} and this value drops to $\sim$19–24 km mol^{-1} at the 6-311++G (3df,3pd) level, i.e., a scaling factor of $f_{\mathrm{ali}} \approx 0.85$. This confirms the need for a non-zero offset in intensity scaling because $f_{\mathrm{ali}} \neq f_{\mathrm{aro}}$.

References

Allamandola, L. J., Tielens, A. G. G. M., & Barker, J. R. 1985, ApJL, 290, L25
Allamandola, L. J., Tielens, A. G. G. M., & Barker, J. R. 1989, ApJS, 71, 733
Alvaro Galué, H., Pirali, O., & Oomens, J. 2010, A&A, 517, A15
Bauschlicher, C. 1998, CP, 233, 29
Bauschlicher, C. 2009, MolPh, 107, 809
Bernstein, M. P., Sandford, S. A., & Allamandola, L. J. 1996, ApJL, 472, L127
Bertie, J. E., & Keefe, C. D. 1994, JChPh, 101, 4610
Cané, E., Miani, A., Palmieri, P., Tarroni, R., & Trombetti, A. 1997, JChPh, 106, 9004
Cané, E., Palmieri, P., Tarroni, R., Trombetti, A., & Handy, N. C. 1996, Gazz. Chim. Ital., 126, 289
Cramer, C. J. 2004, Essentials of Computational Chemistry: Theories and Models (New York: Wiley)
Draine, B. T. 2006, in ASP Conf. Ser. 348, Astrophysics in the Far Ultraviolet: Five Years of Discovery with FUSE, ed. G. Sonneborn, H. Moos, & B.-G. Andersson (San Francisco, CA: ASP), 58
Draine, B. T., & Li, A. 2001, ApJ, 551, 807
Draine, B. T., & Li, A. 2007, ApJ, 657, 810
Frisch, M. J., Trucks, G. W., Schlegel, H. B., et al. 2009, Gaussian 09, Revision B01 (Wallingford, CT: Gaussian, Inc.)
Galabov, B., Ilieva, S., Gounev, T., & Steele, D. 1992, JMoSt, 273, 85
Gao, J., Bouwman, J., Berden, G., & Oomens, J. 2016, JPCA, 120, 7800
Geballe, T. R., Lacy, J. H., Persson, S. E., McGregor, P. J., & Soifer, B. T. 1985, ApJ, 292, 500
Geballe, T. R., Tielens, A. G. G. M., Allamandola, L. J., Moorhouse, A., & Brand, P. W. J. L. 1989, ApJ, 341, 278
Geballe, T. R., Tielens, A. G. G. M., Kwok, S., & Hrivnak, B. J. 1992, ApJL, 387, L89
Gruet, S., Pirali, O., Goubet, M., Tokaryk, D. W., & Brechignac, P. 2016, JPCA, 120, 95
Hudgins, D. M., & Allamandola, L. J. 1995a, JPhCh, 99, 3033
Hudgins, D. M., & Allamandola, L. J. 1995b, JPhCh, 99, 8978
Hudgins, D. M., & Allamandola, L. J. 1997, JPCA, 101, 3472
Hudgins, D. M., Bauschlicher, C. W., Jr., & Allamandola, L. J. 2005, ApJ, 632, 316
Hudgins, D. M., Bauschlicher, C. W., Jr., & Sandford, S. A. 2004, ApJ, 614, 770
Hudgins, D. M., & Sandford, S. A. 1998a, JPCA, 102, 329
Hudgins, D. M., & Sandford, S. A. 1998b, JPCA, 102, 344
Joblin, C., d'Hendecourt, L., Léger, A., & Defourneau, D. 1994, A&A, 281, 923
Joblin, C., Tielens, A. G. G. M., Allamandola, L. J., & Geballe, T. R. 1996, ApJ, 458, 610
Jourdain de Muizon, M., d'Hendecourt, L. B., & Geballe, T. R. 1990, A&A, 235, 367
Jourdain de Muizon, M., Geballe, T. R., d'Hendecourt, L. B., & Baas, F. 1986, ApJL, 306, L105
Kwok, S., & Zhang, Y. 2011, Natur, 479, 80
Léger, A., & Puget, J. 1984, A&A, 137, L5
Li, A. 2004, in ASP Conf. Ser. 309, Astrophysics of Dust, ed. A. N. Witt, G. C. Clayton, & B. T. Draine (San Francisco, CA: ASP), 417
Li, A., & Draine, B. T. 2012, ApJL, 760, L35
Malloci, G., Mulas, G., Cecchi-Pestellini, C., & Joblin, C. 2008, A&A, 489, 1183
Mathis, J. S., Mezger, P. G., & Panagia, N. 1983, A&A, 128, 212
Mattioda, A. L., Rutter, L., Parkhill, J., et al. 2008, ApJ, 680, 1243
Mori, T. I., Onaka, T., Sakon, I., et al. 2014, ApJ, 784, 53
Nagata, T., Tokunaga, A. T., Sellgren, K., et al. 1988, ApJ, 326, 157
Onaka, T., Mori, T. I., Sakon, I., et al. 2014, ApJ, 780, 114
Pavlyuchko, A. I., Vasilyev, E. V., & Gribov, L. A. 2012, JApSp, 78, 782
Peeters, E. 2014, in IAU Symp. 297, The Diffuse Interstellar Bands, ed. J. Cami & N. L. J. Cox (Cambridge: Cambridge Univ. Press), 187
Peeters, E., Allamandola, L. J., Hudgins, D. M., Hony, S., & Tielens, A. G. G. M. 2004, in ASP Conf. Ser. 309, Astrophysics of Dust, ed. A. N. Witt, G. C. Clayton, & B. T. Draine (San Francisco, CA: ASP), 141
Pople, J. A., Head-Gordon, M., & Raghavachari, K. 1987, JChPh, 87, 5968
Rouillé, G., Steglich, M., Carpentier, Y., et al. 2012, ApJ, 752, 25
Sandford, S. A. 1991, ApJ, 376, 599
Sandford, S. A., Bernstein, M. P., & Materese, C. K. 2013, ApJS, 205, 8
Simon, A., & Joblin, C. 2010, ApJ, 712, 69
Sloan, G. C., Bregman, J. D., Geballe, T. R., Allamandola, L. J., & Woodward, C. E. 1997, ApJ, 474, 735
Sloan, G. C., Lagadec, E., Zijlstra, A. A., et al. 2014, ApJ, 791, 28
Smith, T. L., Clayton, G. C., & Valencic, L. 2004, AJ, 128, 357

Steglich, M., Jäger, C., Huisken, F., et al. 2013, ApJS, 208, 26
Szczepanski, J., & Vala, M. 1993a, ApJ, 414, 646
Szczepanski, J., & Vala, M. 1993b, Natur, 363, 699
Szczepanski, J., Wang, H., Vala, M., et al. 2006, ApJ, 646, 666
Thrower, J. D., Jørgensen, B., Friis, E. E., et al. 2012, ApJ, 752, 3
Tielens, A. G. G. M., Allamandola, L. J., Barker, J. R., & Cohen, M. 1987, in Polycyclic Aromatic Hydrocarbons and Astrophysics, ed. A. Léger, L. d'Hendecourt, & N. Boccara (Dordrecht: Reidel), 273

Wilmshurst, J. K., & Bernstein, H. J. 1957, Can. J. Chem., 35, 911
Yamagishi, M., Kaneda, H., Ishihara, D., et al. 2012, A&A, 541, A10
Yang, X. J., Glaser, R., Li, A., & Zhong, J. X. 2013, ApJ, 776, 110
Yang, X. J., Glaser, R., Li, A., & Zhong, J. X. 2016a, MNRAS, 462, 1551
Yang, X. J., Glaser, R., Li, A., & Zhong, J. X. 2017, NewAR, in press (arXiv:1702.03438)
Yang, X. J., Li, A., Glaser, R., & Zhong, J. X. 2016b, ApJ, 825, 22
Yu, H. G., & Nyman, J. 2012, ApJ, 751, 3